

A Low-Complexity Channel Estimation in Internet of Vehicles in Intelligent Transportation Systems for 5G Communication

Lichao Yan, School of Intelligent Engineering, Zhengzhou University of Aeronautics, China*

ABSTRACT

The objective of utilizing mmWave/subTHz bands in next-generation wireless communications is to be achieved. Despite this, since reconfigurable intelligent surface (RIS)-assisted systems depend on the transmission channel configuration, the system architecture design, and the methods used to derive channel state information (CSI) on a base station (BS) and RIS, channel estimation continues to be the main problem with these systems. This research proposes an innovative RIS-based and compressed sensing-based channel estimation technique for the internet of vehicles. To obtain the best phase shift matrix, the communication model must first be constructed, and the angle-of-arrival and departure are utilized. Channel estimation is then performed based on the perception matrix. The training overhead and complexity of the channel estimation are reduced by considering the position information of the vehicles in the optimal phase shift matrix. Simulation results show that the proposed algorithm exhibits better channel estimation and low complexity performance compared with existing algorithms.

KEYWORDS

5G Networks, Channel Estimation, Complexity, Intelligent Compressed Sensing, Intelligent Reflecting Surface, Optimization Algorithm, Transportation System, Vehicular Communication

INTRODUCTION

The reconfigurable intelligent surface (RIS) has an endless number of application possibilities in terahertz (THz) (Bakht et al., 2019) and millimeter wave (mmWave) systems (Mohammed et al., 2019; Shahjehan et al., 2020). It offers a low-cost, passively controlled hardware structure (Jabeen et al., 2019). Since its introduction, the concept of RIS has gained immediate acceptance in various fields related to wireless communication (Alsafasfeh et al., 2019). An RIS is composed of digitally adjustable passive reflective elements (Narayanan et al., 2018). The system can modify the incident signal's independent amplitude and/or phase shift to alter the wireless channel used to transport data between the transmitter and receiver (Kotobi et al., 2015). An RIS can therefore modify the wireless propagation environment to enhance signal transmission. Unlike conventional active relay

DOI: 10.4018/JOEUC.326759

*Corresponding Author

This article published as an Open Access article distributed under the terms of the Creative Commons Attribution License (<http://creativecommons.org/licenses/by/4.0/>) which permits unrestricted use, distribution, and production in any medium, provided the author of the original work and original publication source are properly credited.

beamforming, an RIS enables full-duplex passive beamforming reflection (Haykin, 2005; Goldsmith et al., 2009; Zhang et al., 2008) and does not require an active radio frequency chain for signal transmission, reception, and self-interference cancellation.

Additionally, owing to its low profile, light weight, and ability to maintain geometry, it can be deployed flexibly and at scale. The RIS has undergone extensive research and has been integrated into various wireless communication environments, including system throughput (Zhao et al., 2008; Yoo & Goldsmith, 2006; Schubert & Boche, 2004), network coverage (Costello, 2009; Qaisar et al., 2020; Tareq et al., 2020), communication security (Nasif et al., 2021; Abdulameer et al., 2020; Fook et al., 2020), communication rate (Alathamneh, 2019; Yan et al., 2016; An et al., 2018; Wu & Zhang, 2020), and channel estimation (Di et al., 2020; Pan et al., 2020; Zheng, et al., 2021; Ramezani & Jamalipour, 2021). This is due to the aforementioned performance attributes of the RIS.

Each passive reflecting element in the uniform planar array of the RIS can slightly alter the amplitude and phase of the incident signal, greatly controlling the signal's direction and strength at the receiving end (Han, et al., 2022). This feature enables the RIS to assist the system in building an intelligent and reliable edge intelligence system with a higher degree of freedom by helping the system enhance or suppress directional signals according to the needs of each edge agent and forming a fine-grained, three-dimensional passive beam that meets those needs (Hilo et al., 2022; Dong et al., 2021). The RIS has a regulated wireless environment and a collaborative mechanism to allocate resources precisely and effectively. Studies have shown that this technique may significantly enhance the performance of the system in RIS-assisted multiple-input multiple-output (MIMO) systems (Taghavi et al., 2021; Shen, et al., 2021), IRS-assisted orthogonal frequency division multiplexing (OFDM) systems (Li, et al., 2022), IRS-assisted non-orthogonal multiple access (NOMA) systems (Liu et al., 2021), and other systems. Feng et al. (2021) provided a detailed description of IRS-assisted wireless networks, including their key wireless communications applications, benefits over competing technologies, hardware architecture, beamforming design, channel estimation, and network implementation. In terms of theoretical study on data aggregation, Sun & Yan (2021) suggested that to achieve ultra-high-speed data aggregation, the performance of the wireless computing (AirComp) system should be enhanced by deploying IRS. To fully exploit the benefits of the AirComp system, Zheng et al. (2021) recommended integrating IRS into the large-scale cloud radio access network (C-RAN).

The key aspect in improving system transmission performance in the wireless communication environment is the design of the RIS phase-shift beam. However, because of the large number of RIS reflecting components, getting thorough channel state information (CSI) is often essential, resulting in a considerable training overhead to construct an appropriate RIS phase-shifted beam using the conventional design framework. Instant CSI is employed in each of the aforementioned studies. A second link needs to be built for frequent data exchange between the transceiver and RIS, thereby increasing hardware costs. The phase shift design of the transmitting beam and RIS exclusively relies on statistics derived from position information, and relative location data of the communication devices can be easily acquired through the IoV system during communication. Consequently, combining RIS with the IoV has three advantages:

1. Statistical CSI (Xu et al., 2022) based on location data reduces training expenses.
2. Regular updates are not required because location data change much more slowly than instantaneous CSI.
3. Because only a small amount of location data need to be shared between users, base stations, and RIS, only low-capacity lines are required, thereby reducing hardware costs.

However, applying RIS in the IoV presents additional challenges. First, the signal is affected by a Doppler frequency shift during reception owing to the movement of the vehicle, necessitating a

matching Doppler correction at the RIS end. Second, the positioning performance has inherent errors that further increase the computational complexity of the channel estimate.

For the channel estimation problem of IRS-assisted communication, He et al. (2021) adopted row-column block sparsity to jointly estimate the cascaded channel properties and formulate the multi-user joint sparse matrix recovery problem based on multiple measurement vectors. However, the optimization variables are usually coupled in the non-convex and hard-to-solve simulated multiuser joint sparse matrix recovery problem. A method based on substitution optimization and iterative weighting algorithm can effectively solve the problem. Zhenqing et al. (2020) used a sparse matrix decomposition algorithm based on bilinear generalized approximate message passing (BiG-AMP) to solve the sparse problem of the channel and the Riemann gradient algorithm to achieve sparse matrix completion. However, the performance of this algorithm deteriorates as the number of random variables estimated in the sparse matrix factorization stage increases.

On the other hand, scholars have proposed the bilinear adaptive vector approximate message passing algorithm (BAAdvAMP) (Mirza et al., 2021) for IRS channel estimation. This algorithm outperforms the BiG-AMP algorithm. When a user performs channel estimation on sparse channels, compressive sensing algorithms can generally be used (Wang et al., 2021; Tsai et al., 2018). Taha et al. (2021) used compressive sensing and deep learning to control the IRS unit connected to the controller and estimate all channels passing through the IRS unit. Liu et al. (2020) combined the compressed sensing algorithm with the AMP algorithm to perform channel estimation on the IRS-assisted concatenated channel. In an IRS-assisted communication system, optimized linear precoding (Nadeem et al., 2020) and iterative (Zhang et al., 2020) algorithms are also methods for solving channel estimation. In millimeter wave communication systems, researchers have proposed the use of beam search (Tan et al., 2018) in IRS-assisted millimeter wave networks to find the best beam for the desired user, thereby enhancing the channel quality of the millimeter wave. However, none of the above algorithms has explored the channel estimation problem in the IRS-assisted millimeter wave communication system. In this paper we study the channel estimation problem in this system environment.

Our research explored easily accessible location information based on IoV and proposed a location-based assisted compressed sensing channel estimation method. By establishing a system model based on the relative location data of the sender, receiver, and RIS, we demonstrated that the optimal phase shift information of the RIS has a lower computational cost compared with the conventional CVX convex optimization toolbox for solving suboptimal RIS phase shift information.

The main contributions of this study are as follows:

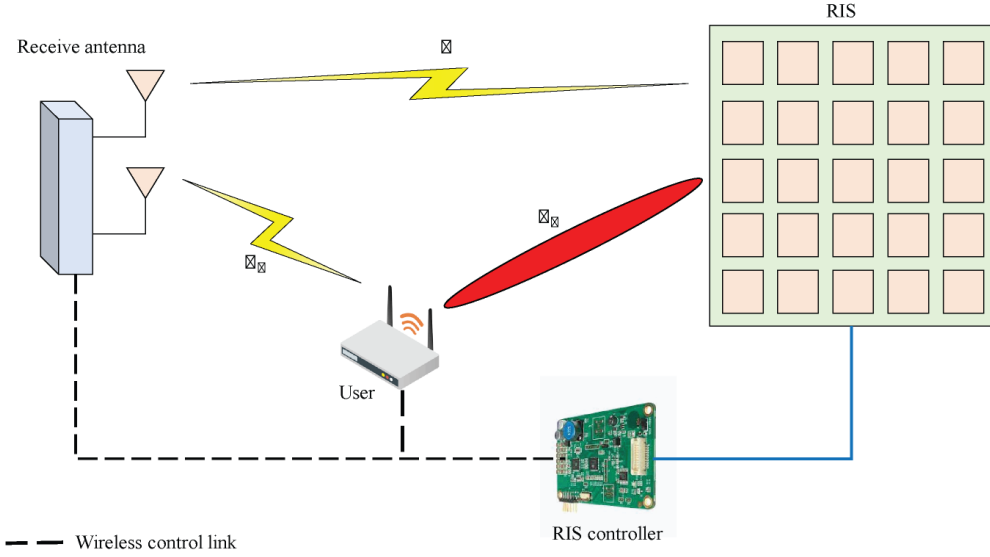
- This work creates a sensing matrix that satisfies the desired channel function using compressed sensing theory and the resulting phase shift matrix.
- According to the analysis of simulation data for the proposed algorithm, the Orthogonal Matching Pursuit (OMP) approach demonstrates better channel estimation performance compared with the classical compressive sensing technique.

Symbol description: In this paper, lowercase \mathbf{a} and uppercase \mathbf{A} bold letters represent vector and matrix, respectively; \mathbf{A}^T and \mathbf{A}^H represent the transpose and conjugate transpose of matrix \mathbf{A} , respectively; $\text{diag}(x)$ represents the diagonal matrix of vector x ; \otimes represents the Kronecker product; and \mathbf{A}_F represents the Frobenius norm of matrix \mathbf{A} .

SYSTEM MODEL

This section provides a detailed introduction to the uplink communication process of the wireless communication system with RIS assistance, as depicted in Figure 1. It focuses on the user's interaction

Figure 1. Proposed system model



with the RIS system and the receiving antenna in a single-user situation. The RIS reflecting components are organized in an N uniform planar array (UPA), and there are M receiving antennas.

The location coordinates of the BS, RIS, and single-antenna user in the wireless communication environment are determined based on the IoV system as shown in equation (1):

$$\begin{cases} BS : (x_B, y_B, z_B) \\ RIS : (x_R, y_R, z_R) \\ User : (x_U, y_U, z_U) \end{cases} \quad (1)$$

The provided coordinates are the center point locations of the respective communication units. The azimuth and elevation angles of the BS receiving signal in the wireless channel from RIS to BS can be respectively determined using the formula shown in equation (2):

$$\begin{cases} \gamma^{G_i} = \arcsin \left(\frac{x_R - x_B}{\sqrt{(y_R - y_B)^2 + (x_R - x_B)^2}} \right) \\ \varphi^{G_i} = \arcsin \left(\frac{z_R - z_B}{\sqrt{(z_R - z_B)^2 + (y_R - y_B)^2 + (x_R - x_B)^2}} \right) \end{cases} \quad (2)$$

The reflected signal in the wireless channel from RIS to BS has the following azimuth and elevation angles, respectively, as shown in equation (3):

$$\left\{ \begin{array}{l} \gamma^{G_r} = \arcsin \left(\frac{x_B - x_R}{\sqrt{(y_R - y_B)^2 + (x_R - x_B)^2}} \right) \\ \varphi^{G_r} = \arcsin \left(\frac{z_B - z_R}{\sqrt{(z_R - z_B)^2 + (y_R - y_B)^2 + (x_R - x_B)^2}} \right) \end{array} \right. \quad (3)$$

As shown in equation (4), the RIS incident signal's azimuth and elevation angles in the wireless channel from User to RIS are, respectively:

$$\left\{ \begin{array}{l} \gamma^t = \arcsin \left(\frac{x_U - x_R}{\sqrt{(y_U - y_B)^2 + (x_U - x_B)^2}} \right) \\ \varphi^t = \arcsin \left(\frac{z_U - z_R}{\sqrt{(z_U - z_B)^2 + (y_U - y_B)^2 + (x_U - x_B)^2}} \right) \end{array} \right. \quad (4)$$

As shown in equation (5), the concatenated channels G from BS to RIS and h_t from RIS to the receiving end are first created based on equations (2) and (4), specifically:

$$\left\{ \begin{array}{l} G = \sqrt{MN} \alpha^G b(\gamma^{G_t}, \varphi^{G_t}) a(\gamma^{G_r}, \varphi^{G_r})^T \\ \mathbf{h}_t = \sqrt{N} \alpha^t a(\gamma^t, \varphi^t) \end{array} \right. \quad (5)$$

In this equation, α^G denotes the path loss from the receiving end to the RIS, while α^t denotes the path loss from the RIS to the broadcasting end. M and N denote the number of base station antennas and the number of RIS reflection elements, respectively. In addition, $a(\gamma, \varphi)$ and $b(\gamma, \varphi)$ can be written as shown in equation (6):

$$\left\{ \begin{array}{l} a(\gamma, \varphi) = \frac{1}{\sqrt{N}} \left[e^{-j\frac{2\pi}{\lambda} d \sin(\gamma) \cos(\varphi) n_1} \right] \otimes \left[e^{-j\frac{2\pi}{\lambda} d \sin(\varphi) n_2} \right] \\ b(\gamma, \varphi) = \frac{1}{\sqrt{M}} \left[e^{-j\frac{2\pi}{\lambda} d \sin(\gamma) \cos(\varphi) m_1} \right] \otimes \left[e^{-j\frac{2\pi}{\lambda} d \sin(\varphi) m_2} \right] \end{array} \right. \quad (6)$$

In equation (6), γ and φ represent the azimuth and elevation angles of the signal, respectively, and the formula $n_1 = n_2 = [0, 1, \dots, \sqrt{N} - 1]$, $m_1 = m_2 = [0, 1, \dots, \sqrt{M} - 1]$, λ is the wavelength. The antenna spacing is set to $d = \lambda / 2$ to simplify the calculation.

The user's $M \times N$ cascaded channel is defined as $H \triangleq G \text{diag}(\mathbf{h}_t)$, which is then expressed in virtual angle domain and written as shown in equation (7):

$$\mathbf{H} = \mathbf{U}_M \tilde{\mathbf{H}} \mathbf{U}_N^T \quad (7)$$

In equation (7), \mathbf{U}_M and \mathbf{U}_N stand for unitary matrices of order $M \times M$ on BS and $N \times N$ dictionary unitary matrices on RIS, respectively. $\tilde{\mathbf{H}}$ represents the $M \times N$ concatenated channel in the angular domain. It displays sparsity because there aren't many scatterers close to BS and RIS. Conventional channel estimation techniques may be used to obtain the direct route parameters from the BS to the user. The cascaded channel's estimation problem is the primary focus of this study. All transmitting end users pass through RIS in the Q time slots using the commonly employed orthogonal pilot transmission technique. For uplink channel estimation, the base station receives the known pilot channel.

After the user disregards the direct path channel, the effective received signal \mathbf{Y}_q in the q -th time slot ($q = 1, 2, \dots, Q$) may be stated as shown in equation (8):

$$\mathbf{Y}_q = \mathbf{G} \text{diag}(\theta_q) \mathbf{h}_t \mathbf{s}_q + \mathbf{z}_q = \mathbf{G} \text{diag}(\mathbf{h}_t) \theta_q \mathbf{s}_q + \mathbf{z}_q \quad (8)$$

In this equation, \mathbf{s}_q represents the pilot signal sent by the BS in the q -th time slot, $\theta_q = [\theta_{q,1}, \theta_{q,2}, \dots, \theta_{q,N}]^T$ represents the $N \times 1$ reflection vector at the RIS, $\theta_{q,n}$ represents the n -th reflection coefficient matrix of ($n = 1, \dots, N$) RIS reflective elements in the q -th time slot, and \mathbf{z}_q represents the user interface in the q -th time slot additive white Gaussian noise with zero mean and variance σ^2 at the receiving end. From the concatenated channel $\mathbf{H} \triangleq \mathbf{G} \text{diag}(\mathbf{h}_t)$, equation (8) can be further written as shown in equation (9):

$$\mathbf{Y}_q = \mathbf{H} \theta_q \mathbf{s}_q + \mathbf{z}_q \quad (9)$$

After the pilot transmission of Q slots, the $M \times Q$ measurement matrix $\mathbf{Y} = [\mathbf{Y}_1, \mathbf{Y}_2, \dots, \mathbf{Y}_Q]$ is obtained. Assuming $s_q = 1$, the measurement matrix can be obtained from equation (7) as shown in equation (10):

$$\mathbf{Y} = \mathbf{H} \Theta + \mathbf{Z} = \mathbf{U}_M \tilde{\mathbf{H}} \mathbf{U}_N^T \Theta + \mathbf{Z} \quad (10)$$

In equation (10), $\Theta = [\theta_1, \theta_2, \dots, \theta_Q]$ and $\mathbf{Z} = [z_1, z_2, \dots, z_Q]$. Define $\tilde{\mathbf{Y}}_q = (\mathbf{U}_M^H \mathbf{Y}_q)^H$ to be the effective measurement matrix of $Q \times M$, and $\tilde{\mathbf{Z}} = (\mathbf{U}_M^H \mathbf{Z})^H$ to be the effective noise matrix of $Q \times M$. Based on the compressed sensing model (Liu & Jia, 2020), equation (10) can be written as shown in equation (11):

$$\tilde{\mathbf{Y}} = \tilde{\Theta} \tilde{\mathbf{H}}^H + \tilde{\mathbf{Z}} \quad (11)$$

In this equation, $\tilde{\Theta} = (\mathbf{U}_N^T \Theta)^H$ is the perceptual matrix of order $Q \times N$. The RIS phase shift matrix can be solved using the CVX toolkit based on equations (5) and (11), as detailed in the

derivation procedure in Appendix A. However, the computational complexity of this approach is too high. An all-around RIS phase shift matrix may also be used to generate a perception matrix, although there are some concerns regarding the accuracy of the channel estimation. The computational complexity of this approach increases with the number of RIS components.

CHANNEL MODEL AND PROPOSED ALGORITHM

The optimal reflection coefficient of each unit of the RIS is derived in this section after first revealing the structural sparsity of the cascaded channel in the angle domain and combining it with the readily available position information in the IoV. Based on this, a channel estimation technique that compresses the channel codebook is presented. The suggested channel estimation technique is less computationally demanding than previous channel estimation schemes.

Angle Domain Cascaded Channel

The angle-domain cascaded channel in equation (7) can be further expressed as shown in equation (12):

$$\tilde{\mathbf{H}} = \sqrt{MN}\alpha^G\alpha^t\tilde{\mathbf{b}}\left(\gamma^{G_i},\varphi^{G_i}\right)\tilde{\mathbf{a}}^T\left(\gamma^{G_r},\gamma^t,\varphi^{G_r}+\varphi^t\right) \quad (12)$$

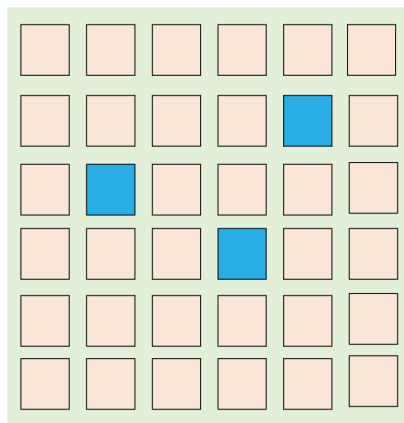
In equation (12), $\tilde{\mathbf{H}}$ is a matrix of order $M \times N$:

$$\tilde{\mathbf{b}}\left(\gamma^{G_i},\varphi^{G_i}\right)=\mathbf{U}_M^H\mathbf{b}\left(\gamma^{G_i},\varphi^{G_i}\right),\tilde{\mathbf{a}}\left(\gamma^t,\varphi^t\right)=\mathbf{U}_N^H\mathbf{a}\left(\gamma^t,\varphi^t\right)$$

and has the location of the array steering vector in the direction of (γ,φ) . \mathbf{U}_M and \mathbf{U}_N have non-zero elements. According to equation (12), a full reflection path can provide $\tilde{\mathbf{H}}$ a non-zero element whose column index relies on $(\gamma^{G_r}+\gamma^t,\varphi^{G_r}+\varphi^t)$ and whose row index depends on $(\gamma^{G_i},\varphi^{G_i})$.

The number of multipaths that the system takes into consideration is correlated with the sparsity of the cascaded channel in the angle domain. Only three RIS reflecting elements, represented by the gray squares in Figure 2, reflect the incident signal during information transmission. As a result, there are only three active channels for the RIS auxiliary system in the cascaded channel.

Figure 2. Sparsity of angle-domain cascaded channels



Algorithm Description

The initial phase shift matrix of the RIS is obtained using the location data in the IoV based on the highest signal power criterion at the receiving end. A compressed sensing-based channel estimation technique is then suggested.

The objective function based on maximum signal strength at the receiving end for the received signal \mathbf{Y}_q at the q -th time slot ($q = 1, 2, \dots, Q$) is given by the formula show in equation (13):

$$\max_{\theta} \left| \mathbf{G} \text{diag}(\mathbf{h}_t) \theta_{q,s} \right|, \text{ s.t. } 0 \leq \theta_{q,n} \leq 2\pi, \forall n = 1, 2, \dots, N \quad (13)$$

Based on location information, determining the phase shift of each RIS component is possible. The phase shift of each RIS reflective element in the q -th time slot can be expressed as $\theta_{q,r,c}$, where (r, c) denotes the r -th position of the corresponding RIS element in column c of the row. According to the constructed system model, $\theta_{q,r,c}$ the formula is expressed as shown in equation (14):

$$\theta_{q,r,c} = \frac{2\pi d}{\lambda} \left(r \left(\sin \gamma^t \sin \varphi^t - \sin \gamma^{G_r} \sin \varphi^{G_r} \right) + c \left(\cos \varphi^t - \cos \varphi^{G_t} \right) \right) \quad (14)$$

In equation (14), $r, c \in 0, 1, \dots, \sqrt{N} - 1$ is the r -th row and c -th column, and γ^t and φ^t are the azimuth and elevation angles of the receiving signal calculated by equation (3), whereas γ^{G_r} , and φ^{G_r} are the azimuth and elevation angles of the reflected signal calculated by equation (4). The specific derivation process is detailed in Appendix B. In addition, the position (r, c) of the RIS element transmitting the signal in the q -th time slot is retrieved, set, and merged with the position information discovered by the IoV system, as shown in equations (15) and (16):

$$t_1 = \sin \gamma^t \sin \varphi^t - \sin \gamma^{G_r} \sin \varphi^{G_r} \quad (15)$$

$$t_2 = \cos \varphi^t - \cos \varphi^{G_r} \quad (16)$$

From t_1 and t_2 , the values of $\mathbf{D}_1, \mathbf{D}_2$, and \mathbf{D}_3 can be further obtained, as shown in equations (17)–(19):

$$\mathbf{D}_1 = \frac{1}{\sqrt{\sqrt{N}}} e^{-j2\pi d(0,1,2,\dots,\sqrt{N}-1)^T(1,1,\dots,1)t_1} \quad (17)$$

$$\mathbf{D}_2 = \frac{1}{\sqrt{\sqrt{N}}} e^{-j2\pi d(0,1,2,\dots,\sqrt{N}-1)^T(1,1,\dots,1)t_2} \quad (18)$$

$$\mathbf{D} = \mathbf{D}_1 \otimes \mathbf{D}_2 \quad (19)$$

After we constructed the training dictionary matrix \mathbf{D} , we needed to construct an $N \times q$ RIS reflection coefficient matrix to match the size of the channel under each time slot q , as shown in equation (20):

$$\Theta_q = \frac{1}{\sqrt{N}} \mathbf{N}(N, q) \quad (20)$$

In this equation, $\mathbf{N}(N, q)$ denotes a $N \times q$ matrix of all 1s, and Θ_q is the reflection coefficient matrix of the N elements in the q -th time slot of the RIS. The dictionary matrix \mathbf{D} and the RIS reflection coefficient matrix Θ_q are combined to create the perception matrix \mathbf{A}_q for the q -th time slot, and the received signal is used to estimate the channel, as shown in equation (21):

$$\mathbf{A}_q = (\mathbf{D}\Theta_q)^H \quad (21)$$

Based on the above formulations, this part of algorithm examines the issue of location information accuracy, primarily focusing on the accuracy of the dictionary matrix solution in the presence of location information inaccuracy. To address this issue, it is primarily coupled with equations (15) and (16); namely, the formulas shown in equations (22) and (23):

$$\mathbf{T}_1 = \mathbf{R}_n t_1 \quad (22)$$

$$\mathbf{T}_2 = \mathbf{R}_n t_2 \quad (23)$$

In these equations, \mathbf{R}_n can be expressed as shown in equation (24):

$$\mathbf{R}_n = \left[1 - \chi : \frac{\chi}{\eta} : 1 + \chi \right] \quad (24)$$

In equation (24), η is the granularity of the error, and χ is influenced by the magnitude of the position error; i.e., $\chi = \varsigma / d_{\text{UR}}$, where ς is the position error and d_{UR} is the positional separation between the user and the RIS. \mathbf{T}_1 and \mathbf{T}_2 can be used to further deduce as shown in equations (25)–(27):

$$\Gamma_{1k} = \frac{1}{\sqrt{\sqrt{N}}} e^{-j2\pi d(0,1,\dots,\sqrt{N}-1)^T(1,1,\dots,1)\mathbf{T}_1(k)} \quad (25)$$

$$\Gamma_{2k} = \frac{1}{\sqrt{\sqrt{N}}} e^{-j2\pi d(0,1,\dots,\sqrt{N}-1)^T(1,1,\dots,1)T_2(k)} \quad (26)$$

$$\Gamma_k = \Gamma_{1k} \otimes \Gamma_{2k} \quad (27)$$

Because T_1 and T_2 are matrices of order $1 \times (2\varphi + 1)$, equations (25)–(27) must be applied sequentially after extracting the k -th value of the error information, $k \in (1, 2\varphi + 1)$. A new perception matrix $A_q^{\Gamma_k}$ can be created based on equation (21) using the error dictionary matrix Γ_k and the RIS reflection vector matrix Θ_q .

In conjunction with equation (11), the maximum row \tilde{t} of the amplitude modulus is calculated using the correlation between the received signal \tilde{Y}_q in the q -th time slot and the perception matrix A_q as shown in equation (28):

$$\tilde{t} = \arg \max A_q \tilde{Y}_q \quad (28)$$

The sensing matrix and the signal received during the time slot are computed in accordance with the maximum row \tilde{t} acquired to directly determine the estimated channel \tilde{H}_e , specifically as shown in equation (29):

$$\begin{cases} R = A_q(:, \tilde{t}) \\ \tilde{H}_e = \text{zeros}(N, 1) \\ \tilde{H}_e(t, :) = (R^T R)^{-1} R \tilde{Y} \end{cases} \quad (29)$$

The specific procedure of the proposed compressed sensing with location aware (CSLA) algorithm is described in Algorithm 1 in accordance with the aforementioned derivation.

Complexity Analysis

The complexity of the suggested CSLA algorithm is thoroughly explained in this section. First, the computational complexity of the estimated matrix is $O(KQN)$ based on the solved perception matrix A , whereas the computational complexity of the RIS reflection phase matrix is $O(KMN^2)$ based on the position information. As a result, the computational complexity of the suggested algorithm is $O(KMN^2) + O(KQN)$. Direct channel estimation has a computational cost of $O(KQMN^2)$ when compared with the conventional compressive sensing approach, assuming a random phase shift matrix that matches the information of the phase shift matrix. Thus, the suggested algorithm has a reduced level of computational complexity.

SIMULATION RESULTS

We compared the proposed CSLA method with the currently widely used channel estimation techniques. We also investigated how changes in system parameters affect channel estimation,

Algorithm 1. CSLA algorithm

Input: $\text{BS}_{(x_1, y_1, z_1)}, \text{RIS}_{(x_2, y_2, z_2)}, \text{User}_{(x_3, y_3, z_3)}, \tilde{\mathbf{Y}}_k, \forall k = 1, 2, \dots, K$

Output: Estimated channel matrix $\tilde{\mathbf{H}}_k, \forall k$

Initialization: $\tilde{\mathbf{H}}_{ke} = 0_{N \times M}, \forall k = 1, 2, \dots, K$

- 1: for $k = 1, 2, \dots, K$
- 2: According to the relative positions of BS, RIS, and User, calculate the transmission azimuth and elevation angles of wireless signals in the reflective elements
 $\gamma_k^{G_t}, \varphi_k^{G_t}, \gamma_k^{G_r}, \varphi_k^{G_r}, \gamma_k^t, \varphi_k^t$
- 3: Determine the position of the reflective element from the position information, and calculate the reflection phase of the RIS reflective element, $\theta_{r,c}$
- 4: Construct the dictionary matrix \mathbf{D}_k , and construct the RIS reflection coefficient matrix Θ_k' according to the time slot information in step 3
- 5: Construct the perception matrix $\mathbf{A}_k = (\mathbf{D}_k \Theta_k')^H$ from the matrices derived in step 4
- 6: Obtain the maximum semaphore position in the channel according to the sparse characteristics of the channel, $\tilde{t}_k = \arg \max \mathbf{A}_k \mathbf{Y}_k$
- 7: Obtain the optimal solution $\mathbf{R}_k = \mathbf{A}_k(:, \tilde{t}_k)$ in the perception matrix from step 6
- 8: Estimate the channel information at the corresponding position t , $\tilde{\mathbf{H}}_{ke}(\tilde{t}_k, :) = (\mathbf{R}_k^T \mathbf{R}_k)^{-1} \mathbf{R}_k \tilde{\mathbf{Y}}_k$
- 9: $\tilde{\mathbf{H}}_k = \mathbf{U}_M^H \tilde{\mathbf{H}}_{ke} \mathbf{U}_N$
- 10: End for

including how the algorithm performs under various SNR conditions, how far different RISes are from the receiving and transmitting ends, and how many reflection units are present in various RISes. The simulation assumed that there is only one RIS system in the entire communication system, and we configured the simulation model to have only one effective path from the sending end to the receiving end, assuming that the direct link signal transmission is blocked. Table 1 presents the specific simulation settings for the system.

We assessed the system performance throughout the simulation process using the normalized mean square error (NMSE) computed as shown in equation (30):

$$\text{NMSE}(\hat{\mathbf{H}}) = \frac{1}{J} \sum_{j=1}^J \frac{\mathbf{H}_j - \hat{\mathbf{H}}_{jF}}{\mathbf{H}_{jF}} \quad (30)$$

In this equation, \mathbf{H} represents the actual channel information, $\hat{\mathbf{H}}_j$ is the estimation of the concatenated channel for the j -th simulation, and J stands for the number of Monte Carlo simulations.

We compared the proposed CSLA method with the most widely used algorithms at the moment: Traditional CS (Liu & Jia, 2020), traditional OMP (Zhang et al., 2021), CVX toolbox (Djelouat et al., 2022), and Oracle LS (Wei et al., 2018). The simulation settings were as follows: the number of RIS components was 1,616; the distances between the RIS and the transmitter and receiver were $d_{UR} = 100$ m and $d_{RB} = 10$ m, respectively, and the concatenated channel noise power was set to 0.

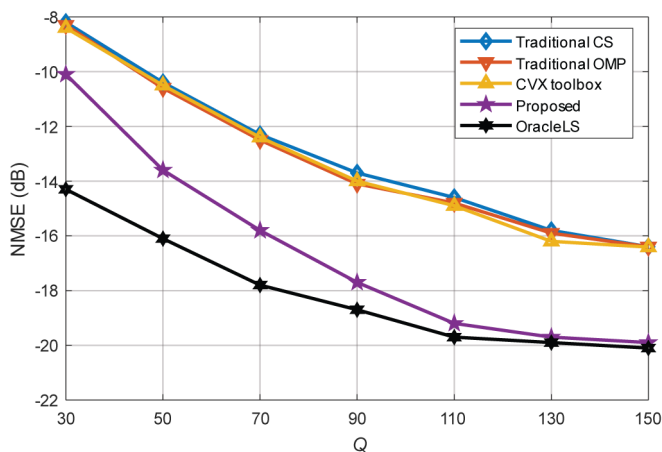
Table 1. Simulation parameters

Parameter	Value
Number of transmitting antennas N_t	1
Number of receiving antennas M	16
Number of RIS reflection elements N	256
Number of launch users K	16
Monte Carlo simulation times	1,000
Transmitter-RIS path loss $ \alpha^t $	$10^{-3} d_{UR}^{-2.2}$
RIS-receiver path loss $ \alpha^r $	$10^{-3} d_{RB}^{-2.8}$
Ranges of AoA and AoD	$-\pi / 2$ to $\pi / 2$

Figure 3 presents the performance comparison between the proposed approach and other algorithms over Q time slots. The Oracle LS technique (Wang et al., 2020) with a known channel and a provided random phase shift matrix was also included in this comparison as a criterion to estimate the channel. The suggested technique outperformed the conventional CS algorithm, the conventional OMP algorithm, and the RIS phase shift based on the CVX toolbox in the same time slot. The suggested algorithm’s performance gain became more noticeable than that of previous techniques as Q increases.

In the simulation process, the location error was set to $\zeta = 1$ m and the error granularity was set to $\eta = 6$ in accordance with the time optimization concept. For the four methods considered in this simulation (CVX toolbox-based, conventional OMP algorithm, proposed methodology, and position error suggested algorithm), the average duration of seven channel estimations was taken into account,

Figure 3. Performance comparison of algorithms in Q timeslots



as shown in Table 2. The following introduces the comprehensive results of the individual channel estimation time.

We executed the algorithm on a Core i5-8300H processor with 8 GB of RAM, a 256GB solid-state drive +1TB HDD, a 1050Ti graphic card, and MATLAB version R2016a. The execution time showed that the suggested CSLA algorithm completed a channel estimation in nearly half the time compared with the conventional OMP technique. When there was a positional information error, the suggested technique would take longer to run as the level of error granularity increased. It saved more time while solving the RIS reflection phase with the OMP method as opposed to using the CVX toolbox. The number of RIS components affected the duration required for various techniques to complete channel estimation. The channel estimation process took longer to complete as the number of RIS components increased.

Given that the number of RIS components affected the system performance, Figure 4 illustrates the NMSE for various RIS component counts. When the transmit power is constant, it is assumed that the ratio of the transmit power to the noise variance at the receiver is 0. The simulation results indicated that the channel estimation performance steadily improved as the number of RIS elements increased, and the NMSE value of the suggested approach was inversely related to the RIS element count.

We analyzed the impact of the number of RIS components on algorithm performance. Figure 5 illustrates the effect of the signal-to-noise ratio (SNR) on the communication system’s performance. In our simulation, the suggested technique outperformed the conventional OMP algorithm at lower SNR levels. The disparity between the NMSE values estimated by the two methods at 9 dB was greater

Table 2. Average time for algorithms to perform seven channel estimations

Algorithm	Time (s)
Based on CVX toolbox	4.877146
Traditional OMP algorithm	0.053092
Proposed CSLA with position error	0.044523
Proposed CSLA without position error	0.036270

Figure 4. NMSE under different numbers of RIS elements

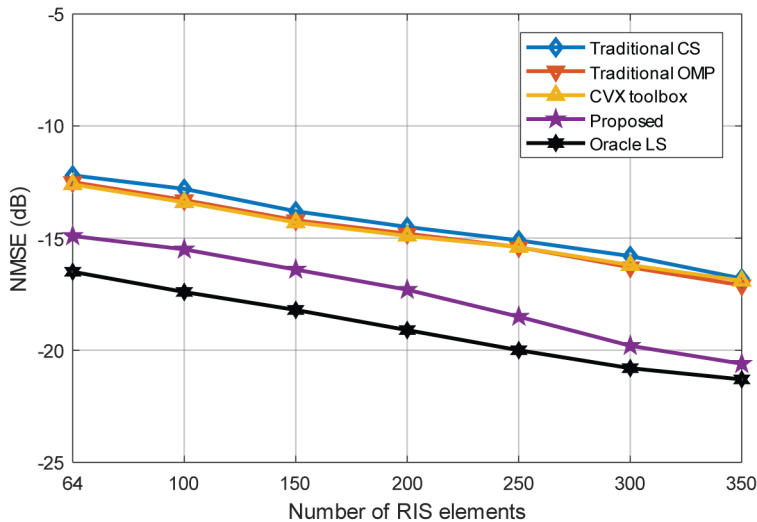
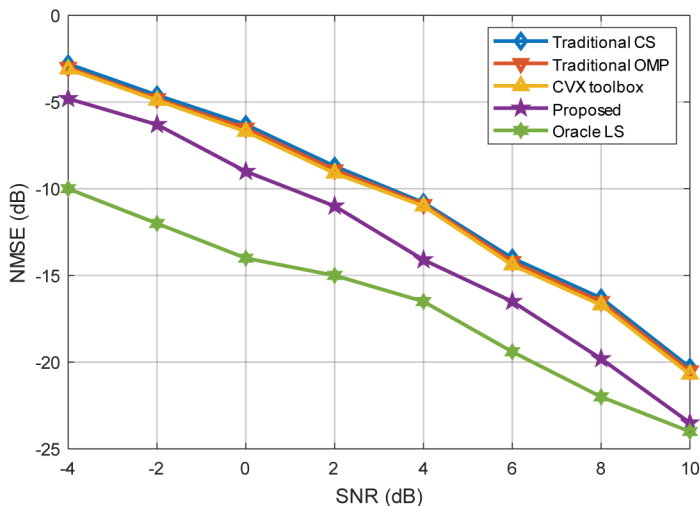


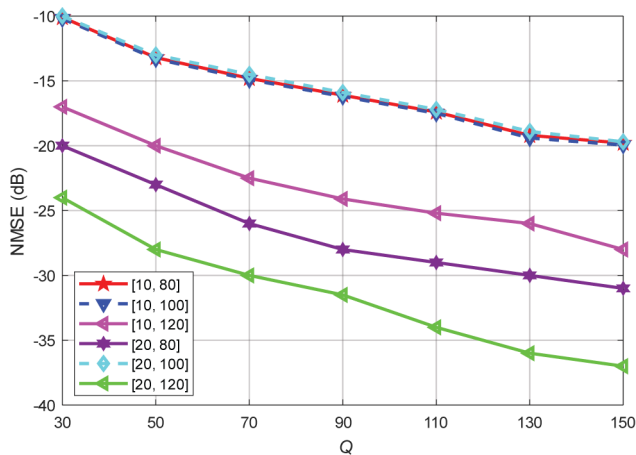
Figure 5. Influence of SNR on channel estimation performance



than that at 5 dB, as evidenced by the comparisons of NMSE values obtained from the proposed and standard OMP algorithms at SNR levels of 5 dB and 9 dB.

For this study we also considered the impact of the distance between the RIS and the transmitter and receiver on the system’s performance, as shown in Figure 6. The figure illustrates how the estimation performance of the system varied under different distance circumstances. For example, when d_{UR} and d_{RB} are [20, 100], [10, 100], and [10, 80], respectively, NMSE did not show much difference in performance. The relative improvement of NMSE when d_{UR} and d_{RB} were [10, 120] was roughly 7 dB. The NMSE increased by around 2 dB when d_{UR} and d_{RB} were [20, 80] in comparison with [10, 120]. The estimation NMSE performance was at its maximum when d_{UR} and d_{RB} were [20, 120], and it increased by around 3 dB when compared with [20, 80]. The simulation

Figure 6. Comparison of channel estimation performance of the proposed algorithm under different values of d_{UR} and d_{RB}



of various d_{UR} and d_{RB} values evinced that the relative position of RIS deployment significantly affected the effectiveness of channel estimation.

CONCLUSION

We investigated the cascaded channel estimation method for a single wireless communication system that uses RIS assistance. Using the relative positions of the transmitter, RIS auxiliary system, and receiver in the IoV, we constructed a 3D model before the RIS auxiliary system was logically deployed in a uniform array. We then calculated the best phase shift for each RIS reflecting unit, considering the maximum signal strength at the receiving end. This calculation created the best RIS phase shift matrix. We then also built the sensing matrix that conforms to the objective channel function based on the ideal phase shift matrix of RIS. Finally, we iteratively calculated the channel information using compressive sensing theory and created the best phase shift matrix based on the collection of position data. This matrix lessened the complexity and extra signaling overhead for cascaded channels. The simulation results showed that the proposed CSLA algorithm exhibited better NMSE performance than other classical channel estimation schemes and offered lower computational complexity when compared with the conventional CS algorithm, the conventional OMP algorithm, and the scheme based on the CVX toolbox for solving the suboptimal RIS phase shift matrix.

Future research should explore the optimal phase shift design problem when a single RIS assists multiple users simultaneously to meet the requirements of enhanced mobile broadband (eMBB) in dense mobile terminal environments, such as shopping malls and stations. These aspects represent the limitations of the current study.

DATA AVAILABILITY

The data used to support the findings of this study are included within the article.

CONFLICTS OF INTEREST

The author declares that there is no conflict of interest regarding the publication of this paper.

FUNDING STATEMENT

This work was supported by Henan Center for Outstanding Overseas Scientists (No. GZS2022011).

REFERENCES

- Abdulameer, A. S., Tiun, S., Sani, N. S., Ayob, M., & Taha, A. Y. (2020). Enhanced clustering models with wiki-based k-nearest neighbors-based representation for web search result clustering. *Journal of King Saud University*, 34(3), 840–850. doi:10.1016/j.jksuci.2020.02.003
- Al-Hilo, A., Samir, M., Elhattab, M., Assi, C., & Sharafeddine, S. (2022). Reconfigurable intelligent surface enabled vehicular communication: Joint user scheduling and passive beamforming. *IEEE Transactions on Vehicular Technology*, 71(3), 2333–2345. doi:10.1109/TVT.2022.3141935
- Alathamneh, G. M., Abdullah, S., & Sani, N. S. (2019). Genetic algorithm selection strategies based rough set for attribute reduction. *International Journal of Computer Science and Network Security*, 19(9), 187–194. http://paper.ijcsns.org/07_book/201909/20190921.pdf
- Alsafasfeh, Q., Saraereh, O. A., Ali, A., Al-Tarawneh, L., Khan, I., & Silva, A. (2019). Efficient power control framework for small-cell heterogeneous networks. *Sensors (Basel)*, 20(5), 1–14. doi:10.3390/s20051467 PMID:32155972
- An, X., Su, J., Lu, X., & Lin, F. (2018). Hypergraph clustering model-based association analysis of DDOS attacks in fog computing intrusion detection system. *EURASIP Journal on Wireless Communications and Networking*, 249(1), 249. Advance online publication. doi:10.1186/s13638-018-1267-2
- Bakht, K., Jameel, F., Ali, Z., Khan, W. U., Khan, I., Sardar Sidhu, G. A., & Lee, J. W. (2019). Power allocation and user assignment scheme for beyond 5G heterogeneous networks. *Wireless Communications and Mobile Computing*, 2019, 1–12. doi:10.1155/2019/2472783
- Costello, D. J. (2009). Fundamentals of wireless communication [Review of the book Fundamentals of wireless communication by David Tse and Pramod Viswanath]. *IEEE Transactions on Information Theory*, 55(2), 919–920. doi:10.1109/TIT.2008.2009814
- Di, B., Zhang, H., Song, L., Li, Y., Han, Z., & Poor, H. V. (2020). Hybrid beamforming for reconfigurable intelligent surface based multi-user communications: Achievable rates with limited discrete phase shifts. *IEEE Journal on Selected Areas in Communications*, 38(8), 1809–1822. doi:10.1109/JSAC.2020.3000813
- Djelouat, H., Leinonen, M., & Juntti, M. (2022). Spatial correlation aware compressed sensing for user activity detection and channel estimation in massive MTC. *IEEE Transactions on Wireless Communications*, 21(8), 6402–6416. doi:10.1109/TWC.2022.3149111
- Dong, L., Wang, H.-M., Bai, J., & Xiao, H. (2021). Double intelligent reflecting surface for secure transmission with inter-surface signal reflection. *IEEE Transactions on Vehicular Technology*, 70(3), 2912–2916. doi:10.1109/TVT.2021.3062059
- Feng, K., Chen, Y., Han, Y., Li, X., & Jin, S. (2021). Passive beamforming design for reconfigurable intelligent surface-aided OFDM: A fractional programming based approach. In *Proceedings of the 2021 IEEE 93rd Vehicular Technology Conference (VTC2021-Spring)* (pp. 1–6). IEEE. doi:10.1109/VTC2021-Spring51267.2021.9449003
- Fook, W. S., Abd Rahman, A. H., Sani, N. S., & Adam, A. (2020). Resource optimisation using multithreading in support vector machine. *International Journal of Advanced Computer Science and Applications*, 11(4), 356–359. doi:10.14569/IJACSA.2020.0110449
- Goldsmith, A., Jafar, S. A., Maric, I., & Srinivasa, S. (2009). Breaking spectrum gridlock with cognitive radios: An information theoretic perspective. *Proceedings of the IEEE*, 97(5), 894–914. doi:10.1109/JPROC.2009.2015717
- Han, Y., Zhang, S., Duan, L., & Zhang, R. (2022). Double-IRS aided MIMO communication under LoS channels: Capacity maximization and scaling. *IEEE Transactions on Communications*, 70(4), 2820–2837. doi:10.1109/TCOMM.2022.3151893
- Haykin, S. (2005). Cognitive-radio: Brain-empowered wireless communications. *IEEE Journal on Selected Areas in Communications*, 23(2), 201–220. doi:10.1109/JSAC.2004.839380
- He, J., Wymeersch, H., & Juntti, M. (2021). Channel estimation for RIS-aided mmWave MIMO systems via atomic norm minimization. *IEEE Transactions on Wireless Communications*, 20(9), 5786–5797. doi:10.1109/TWC.2021.3070064

- He, Z.-Q., & Yuan, X. (2020). Cascaded channel estimation for large intelligent metasurface assisted massive MIMO. *IEEE Wireless Communications Letters*, 9(2), 210–214. doi:10.1109/LWC.2019.2948632
- Jabeen, T., Ali, Z., Khan, W. U., Jameel, F., Khan, I., Sardar Sidhu, G. A., & Choi, B. J. (2019). Joint power allocation and link selection for multi-carrier buffer aided relay network. *Electronics (Basel)*, 8(6), 1–14. doi:10.3390/electronics8060686
- Kotobi, K., Mainwaring, P. B., Tucker, C. S., & Bilen, S. G. (2015). Data-throughput enhancement using data mining-informed cognitive radio. *Electronics (Basel)*, 4(2), 221–238. doi:10.3390/electronics4020221
- Li, Q., Wang, S., & Wang, Y. (2022). Rank-two multicast beamforming for multiuser MISO downlink with intelligent reflecting surface. *IEEE Transactions on Vehicular Technology*, 71(6), 6722–6726. doi:10.1109/TVT.2022.3155971
- Liu, H., Yuan, X., & Zhang, Y.-J. A. (2020). Message-passing based channel estimation for reconfigurable intelligent surface assisted MIMO. In *Proceedings of the 2020 IEEE International Symposium on Information Theory (ISIT)* (pp. 2983–2988). IEEE. doi:10.1109/ISIT44484.2020.9173987
- Liu, P., Li, Y., Cheng, W., Gao, X., & Huang, X. (2021). Intelligent reflecting surface aided NOMA for millimeter-wave massive MIMO with lens antenna array. *IEEE Transactions on Vehicular Technology*, 70(5), 4419–4434. doi:10.1109/TVT.2021.3067938
- Liu, X., & Jia, L. (2020). Deterministic construction of compressed sensing matrices via vector spaces over finite fields. *IEEE Access : Practical Innovations, Open Solutions*, 8, 203301–203308. doi:10.1109/ACCESS.2020.3034912
- Mirza, J., & Ali, B. (2021). Channel estimation method and phase shift design for reconfigurable intelligent surface assisted MIMO networks. *IEEE Transactions on Cognitive Communications and Networking*, 7(2), 441–451. doi:10.1109/TCCN.2021.3072895
- Mohammed, S. L., Alsharif, M. H., Gharghan, S. K., Khan, I., & Albreem, M. (2019). Robust hybrid beamforming scheme for millimeter-wave massive-MIMO 5G wireless networks. *Symmetry*, 11(11), 1–16. doi:10.3390/sym11111424
- Nadeem, Q.-U.-A., Alwazani, H., Kammoun, A., Chaaban, A., Debbah, M., & Alouini, M.-S. (2020). Intelligent reflecting surface-assisted multi-user MISO communication: Channel estimation and beamforming design. *IEEE Open Journal of the Communications Society*, 1, 661–680. doi:10.1109/OJCOMS.2020.2992791
- Narayanan, R. M., Pooler, R. K., Martone, A. F., Gallagher, K. A., & Sherbondy, K. D. (2018). The spectrum analysis solution (SAS) system: Theoretical analysis, hardware design and implementation. *Sensors (Basel)*, 18(2), 1–22. doi:10.3390/s18020652 PMID:29470448
- Nasif, A., Othman, Z. A., & Sani, N. S. (2021). The deep learning solutions on lossless compression methods for alleviating data load on IoT nodes in smart cities. *Sensors (Basel)*, 21(12), 1–23. doi:10.3390/s21124223 PMID:34203024
- Pan, C., Ren, H., Wang, K., Xu, W., Elkashlan, M., Nallanathan, A., & Hanzo, L. (2020). Multicell MIMO communications relying on intelligent reflecting surfaces. *IEEE Transactions on Wireless Communications*, 19(8), 5218–5233. doi:10.1109/TWC.2020.2990766
- Qaisar, Z. H., Irfan, M., Ali, T., Ahmad, A., Ali, G., Glowacz, A., Glowacz, W., Caesarendra, W., Mashraqi, A. M., Draz, U., & Hussain, S. (2020). Effective beamforming technique amid optimal value for wireless communication. *Electronics (Basel)*, 9(11), 1–18. doi:10.3390/electronics9111869
- Ramezani, P., & Jamalipour, A. (2021). Backscatter-assisted wireless powered communication networks empowered by intelligent reflecting surface. *IEEE Transactions on Vehicular Technology*, 70(11), 11908–11922. doi:10.1109/TVT.2021.3116708
- Schubert, M., & Boche, H. (2004). Solution of the multiuser downlink beamforming problem with individual SINR constraints. *IEEE Transactions on Vehicular Technology*, 53(1), 18–28. doi:10.1109/TVT.2003.819629
- Shahjehan, W., Riaz, A., Khan, I., Sadiq, A. S., Khan, S., & Khan, M. K. (2020). Bat algorithm-based beamforming for mmWave massive MIMO systems. *International Journal of Communication Systems*, 33(2), 845–904. doi:10.1002/dac.4182

Shen, H., Xu, W., Gong, S., He, Z., & Zhao, C. (2021). Secrecy rate maximization for intelligent reflecting surface assisted multi-antenna communication. *IEEE Communications Letters*, 23(9), 1488–1492. doi:10.1109/LCOMM.2019.2924214

Sun, S., & Yan, H. (2021). Channel estimation for reconfigurable intelligent surface-assisted wireless communications considering Doppler effect. *IEEE Wireless Communications Letters*, 10(4), 790–794. doi:10.1109/LWC.2020.3044004

Taghavi, E. M., Alizadeh, A., Rajatheva, N., Vu, M., & Latva-aho, M. (2021). User association in millimeter wave cellular networks with intelligent reflecting surfaces. In *Proceedings of the 2021 IEEE 93rd Vehicular Technology Conference (VTC2021-Spring)* (pp. 1–6). IEEE. doi:10.1109/VTC2021-Spring51267.2021.9448951

Taha, A., Alrabeiah, M., & Alkhateeb, A. (2021). Enabling large intelligent surfaces with compressive sensing and deep learning. *IEEE Access : Practical Innovations, Open Solutions*, 9, 44304–44321. doi:10.1109/ACCESS.2021.3064073

Tan, X., Sun, Z., Koutsonikolas, D., & Jornet, J. M. (2018). Enabling indoor mobile millimeter-wave networks based on smart reflect-arrays. *IEEE International Conference on Computer Communication (ICC)*, 270–278. doi:10.1109/INFOCOM.2018.8485924

Tareq, M., Sundararajan, E. A., Mohd, M., & Sani, N. S. (2020). Online clustering of evolving data streams using a density grid-based method. *IEEE Access : Practical Innovations, Open Solutions*, 8, 166472–166490. doi:10.1109/ACCESS.2020.3021684

Tsai, C.-R., Liu, Y.-H., & Wu, A.-Y. (2018). Efficient compressive channel estimation for millimeter-wave large-scale antenna systems. *IEEE Transactions on Signal Processing*, 66(9), 2414–2428. doi:10.1109/TSP.2018.2811742

Wang, P., Fang, J., Duan, H., & Li, H. (2020). Compressed channel estimation for intelligent reflecting surface-assisted millimeter wave systems. *IEEE Signal Processing Letters*, 27(5), 905–909. doi:10.1109/LSP.2020.2998357

Wang, W., & Zhang, W. (2021). Joint beam training and positioning for intelligent reflecting surfaces assisted millimeter wave communications. *IEEE Transactions on Wireless Communications*, 20(10), 6282–6297. doi:10.1109/TWC.2021.3073140

Wei, C., Liu, H., Zhang, Z., Dang, J., & Wu, L. (2018). Near-optimum sparse channel estimation based on least squares and approximate message passing. *IEEE Wireless Communications Letters*, 6(6), 754–757. doi:10.1109/LWC.2017.2739154

Wu, Q., & Zhang, R. (2020). Towards smart and reconfigurable environment: Intelligent reflecting surface aided wireless network. *IEEE Communications Magazine*, 58(1), 106–112. doi:10.1109/MCOM.001.1900107

Xu, W., Zhang, J., Cai, S., Wang, J., & Wu, Y. (2023). RIS-assisted MIMO secure communications with Bob's statistical CSI and without Eve's CSI. *Digital Communications and Networks*, 9(3), 638–644. doi:10.1016/j.dcan.2022.08.008

Yan, Q., Yu, F. R., Gong, Q., & Li, J. (2016). Software-defined networking (SDN) and distributed denial of service (DDoS) attacks in cloud computing environments: A survey, some research issues, and challenges. *IEEE Communications Surveys and Tutorials*, 18(1), 602–622. doi:10.1109/COMST.2015.2487361

Yoo, T., & Goldsmith, A. (2006). On the optimality of multiantenna broadcast scheduling using zero-forcing beamforming. *IEEE Journal on Selected Areas in Communications*, 24(3), 528–541. doi:10.1109/JSAC.2005.862421

Zhang, J., Qi, C., Li, P., & Lu, P. (2020). Channel estimation for reconfigurable intelligent surface aided massive MIMO system. *Proceedings of the 2020 IEEE 21st International Workshop on Signal Processing Advances in Wireless Communications*, 1–5. doi:10.1109/SPAWC48557.2020.9154276

Zhang, L., Liang, Y.-C., & Xin, Y. (2008). Joint beamforming and power allocation for multiple access channels in cognitive radio networks. *IEEE Journal on Selected Areas in Communications*, 26(1), 38–51. doi:10.1109/JSAC.2008.080105

- Zhang, S., Xu, L., & Yan, S. (2021). A low complexity OMP sparse channel estimation algorithm in OFDM system. *Proceedings of the 2021 IEEE International Conference on Signal Processing, Communications and Computing (ICSPCC)*, 1–6. doi:10.1109/ICSPCC52875.2021.9565070
- Zhao, G., Ma, J., Li, Y., Wu, T., Kwon, Y. H., Soong, A., & Yang, C. (2008). Spatial spectrum holes for cognitive radio with directional transmission. In *Proceedings of IEEE GLOBECOM 2008 — the 2008 IEEE Global Telecommunications Conference* (pp. 1–5). IEEE. doi:10.1109/GLOCOM.2008.ECP.582
- Zheng, B., You, C., & Zhang, R. (2021a). Fast channel estimation for IRS-assisted OFDM. *IEEE Wireless Communications Letters*, 10(3), 580–584. doi:10.1109/LWC.2020.3038434
- Zheng, B., You, C., & Zhang, R. (2021b). Uplink channel estimation for double-IRS assisted multi-user MIMO. In *Proceedings of ICC 2021 — IEEE International Conference on Communications* (pp. 1–6). IEEE. doi:10.1109/ICC42927.2021.9501057

APPENDIX A

Solve RIS Phase Shift Matrix by CVX Toolbox

First, construct the objective function, as shown in equation (A1):

$$\max_{\theta} \mathbf{h}_t \Theta G^2, \text{ s.t. } 0 \leq \theta_n \leq 2\pi, \forall n = 1, 2, \dots, N \quad (1)$$

Define $\varepsilon = [\varepsilon_1, \varepsilon_2, \dots, \varepsilon_N]^H$, where $\varepsilon_n = e^{j\theta_n}, \forall n$. To simplify the operation, the element $|\varepsilon_n| = 1$ of the phase shift matrix is defined, and equation (A1) can be transformed into the formula shown in equation (A2):

$$\max_{\varepsilon} \varepsilon^H \Phi \Phi^H \varepsilon, \text{ s.t. } |\varepsilon_n| = 1, \forall n = 1, 2, \dots, N \quad (2)$$

In this equation, $\Phi = \text{diag}(\mathbf{h}_{t,k}) \mathbf{G}$. Define $\mathbf{B} = \Phi \Phi^H$, and further transform equation (A2) into the formula shown in equation (A3):

$$\max_{\varepsilon} \varepsilon^H \mathbf{B} \varepsilon, \text{ s.t. } |\varepsilon_n| = 1, \forall n = 1, 2, \dots, N \quad (3)$$

Note that $\varepsilon^H \mathbf{B} \varepsilon = \text{tr}(\mathbf{B} \varepsilon \varepsilon^H)$, so define $\mathbf{E} = \varepsilon \varepsilon^H$, where \mathbf{E} satisfies $\mathbf{E} \succeq 0$ and $\text{rank}(\mathbf{E}) = 1$, because the rank 1 constraint is non-convex, the problem is solved by positive semi-definite programming; that is, use the formula shown in equation (A4) to solve this problem:

$$\max_{\mathbf{E}} \text{tr}(\mathbf{B} \mathbf{E}), \text{ s.t. } \mathbf{E}_{n,n} = 1, \forall n = 1, 2, \dots, N, \mathbf{E} \succeq 0 \quad (4)$$

The above problem is a standard convex semi-definite program, which can be solved by the CVX toolbox. First, the eigenvalue of \mathbf{E} is obtained, and it is decomposed into $\mathbf{E} = \mathbf{U} \mathbf{D} \mathbf{U}^H$, where $\mathbf{U} = [e_1, e_2, \dots, e_N]$ is a unitary matrix and $\mathbf{D} = \text{diag}(a_1, a_2, \dots, a_N)$ is a diagonal matrix. A suboptimal solution $\varepsilon = \mathbf{U} \sqrt{\mathbf{D}} \mathbf{r}$ is then obtained, where $\mathbf{r} \in \mathbf{C}^{N \times 1}$ is a random vector following a circular symmetric complex Gaussian distribution with zero mean and covariance matrix \mathbf{I}_N . In equation (A3), the target value $\varepsilon = e^{j \arg(\varepsilon(1:N))}$. This method guarantees the approximation of the optimal target value $\pi/4$, but its computational complexity is too large.

APPENDIX B

Derivation Process of $\theta_{q_{r,c}}$

According to equations (5) and (6), the channel vector of RIS-BS corresponding to the reflected signal of the RIS auxiliary system and the channel vector of User-RIS corresponding to the incident signal can be expressed as shown in equation (B1):

$$\begin{cases} \mathbf{h}_{\text{User-RIS}} = \alpha_1 \mathbf{T}_t(\gamma^t, \varphi^t) \\ \mathbf{h}_{\text{RIS-BS}} = \alpha_2 \mathbf{R}_r(\gamma^{G_r}, \varphi^{G_r}) \end{cases} \quad (1)$$

In equation (B1), α_1 and α_2 represent the path loss from User to RIS and the path loss from RIS to BS, respectively. $\mathbf{T}_t(\gamma^t, \varphi^t)$ and $\mathbf{R}_r(\gamma^{G_r}, \varphi^{G_r})$ are defined as shown in equations (B2) and (B3):

$$\mathbf{T}_t(\gamma^t, \varphi^t) = \begin{bmatrix} 1 \dots e^{-j\frac{2\pi d}{\lambda}(r \sin \gamma^t \sin \varphi^t + c \cos \varphi^t)} & \dots e^{-j\frac{2\pi d}{\lambda}((\sqrt{N}-1) \sin \gamma^t \sin \varphi^t + (\sqrt{N}-1) \cos \varphi^t)} \end{bmatrix} \quad (2)$$

$$\mathbf{R}_r(\gamma^{G_r}, \varphi^{G_r}) = \begin{bmatrix} 1 \dots e^{j\frac{2\pi d}{\lambda}(r \sin \gamma^{G_r} \sin \varphi^{G_r} + c \cos \varphi^{G_r})} & \dots e^{j\frac{2\pi d}{\lambda}((\sqrt{N}-1) \sin \gamma^{G_r} \sin \varphi^{G_r} + (\sqrt{N}-1) \cos \varphi^{G_r})} \end{bmatrix} \quad (3)$$

In these equations, γ^{G_r} , φ^{G_r} , γ^t , and φ^t are defined with reference to equations (3) and (4), N represents the number of reflective elements in the RIS system, r is the row index, and c is the column index of the reflector in the RIS surface array unit. In $\mathbf{h}_{\text{User-RIS}}$ and $\mathbf{h}_{\text{RIS-BS}}$, the values of α_1 and α_2 are set to 1 for simplicity. Under the criterion of maximum power at the receiving end, the objective function is defined as shown in equation (B4):

$$\max_{\theta} \mathbf{h}_{\text{User-RIS}} \theta \mathbf{h}_{\text{RIS-BS}}^T \quad (4)$$

When there is no RIS auxiliary system, the phase shift matrix θ is defined as the identity matrix, and the objective function is calculated as shown in equation (B5):

$$\begin{aligned} \mathbf{T}_t(\gamma^t, \varphi^t) \theta \mathbf{R}_r^T(\gamma^{G_r}, \varphi^{G_r}) &= \mathbf{T}_t(\gamma^t, \varphi^t) \begin{bmatrix} 1 & 0 & 0 & 0 \\ 0 & 1 & 1 & 0 \\ \vdots & \vdots & \dots & \dots \\ 0 & 0 & \dots & 1 \end{bmatrix} \mathbf{R}_r^T(\gamma^{G_r}, \varphi^{G_r}) \\ &= 1 + 2 + \dots + e^{j\frac{2\pi d}{\lambda}(r(\sin \gamma^{G_r} \sin \varphi^{G_r} - \sin \gamma^t \sin \varphi^t) + c(\cos \varphi^{G_r} - \cos \varphi^t))} \\ &+ \dots + e^{j\frac{2\pi d}{\lambda}((\sqrt{N}-1)(\sin \gamma^{G_r} \sin \varphi^{G_r} - \sin \gamma^t \sin \varphi^t) + (\sqrt{N}-1)(\cos \varphi^{G_r} - \cos \varphi^t))} \end{aligned} \quad (5)$$